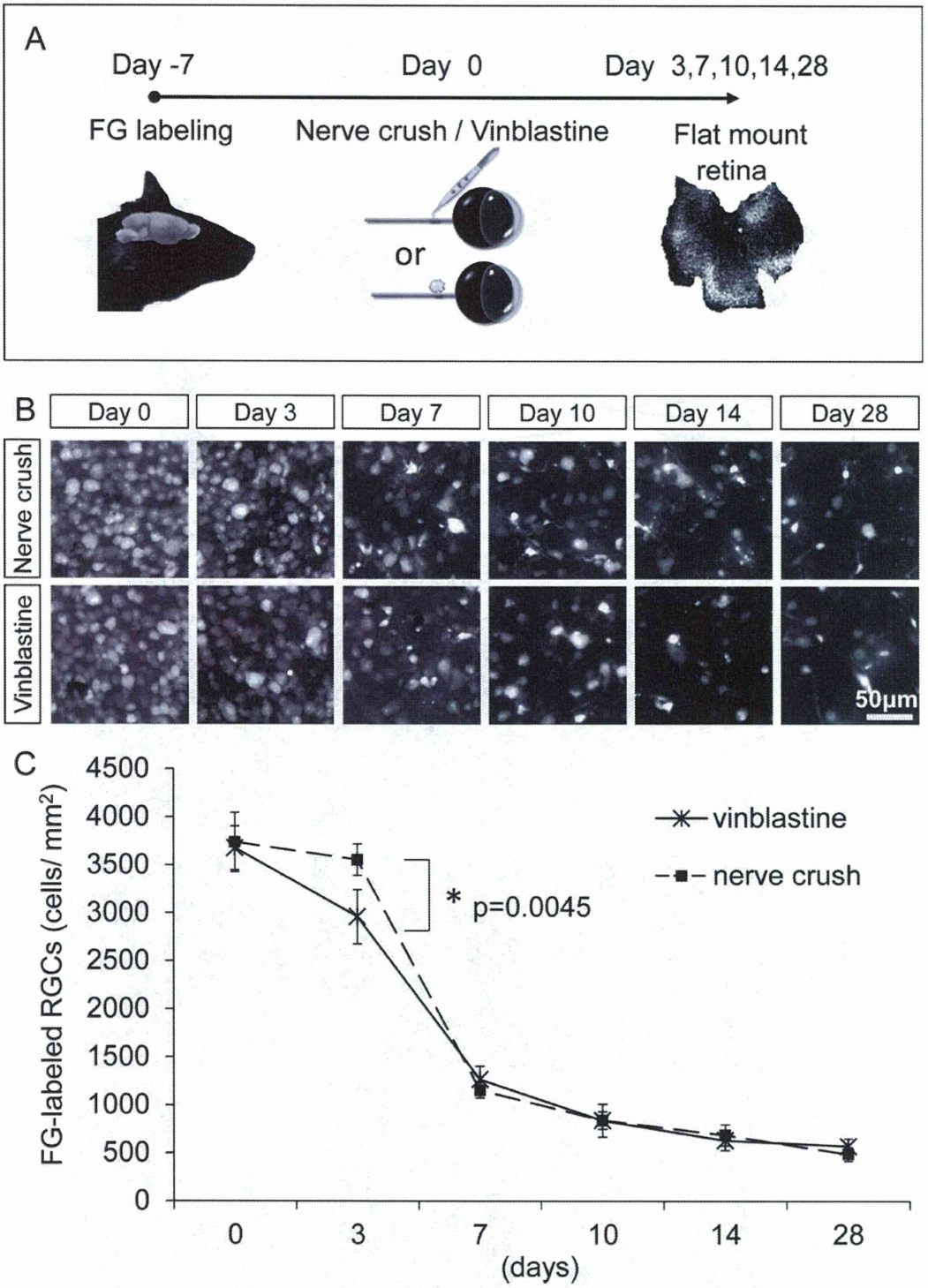

Fig. 3. Time course of RGC death induced by axonal damage. **A:** Schematic diagram of axonal injury-induced RGC death. **B:** Representative appearances of FG-labeled RGCs on the flat-mounted retina at various time points (0, 3, 7, 10, 14, and 28 days) after nerve crush (upper panels) or vinblastine treatment (lower panels). **C:** Quantitative data on FG-labeled RGC following axonal injury.

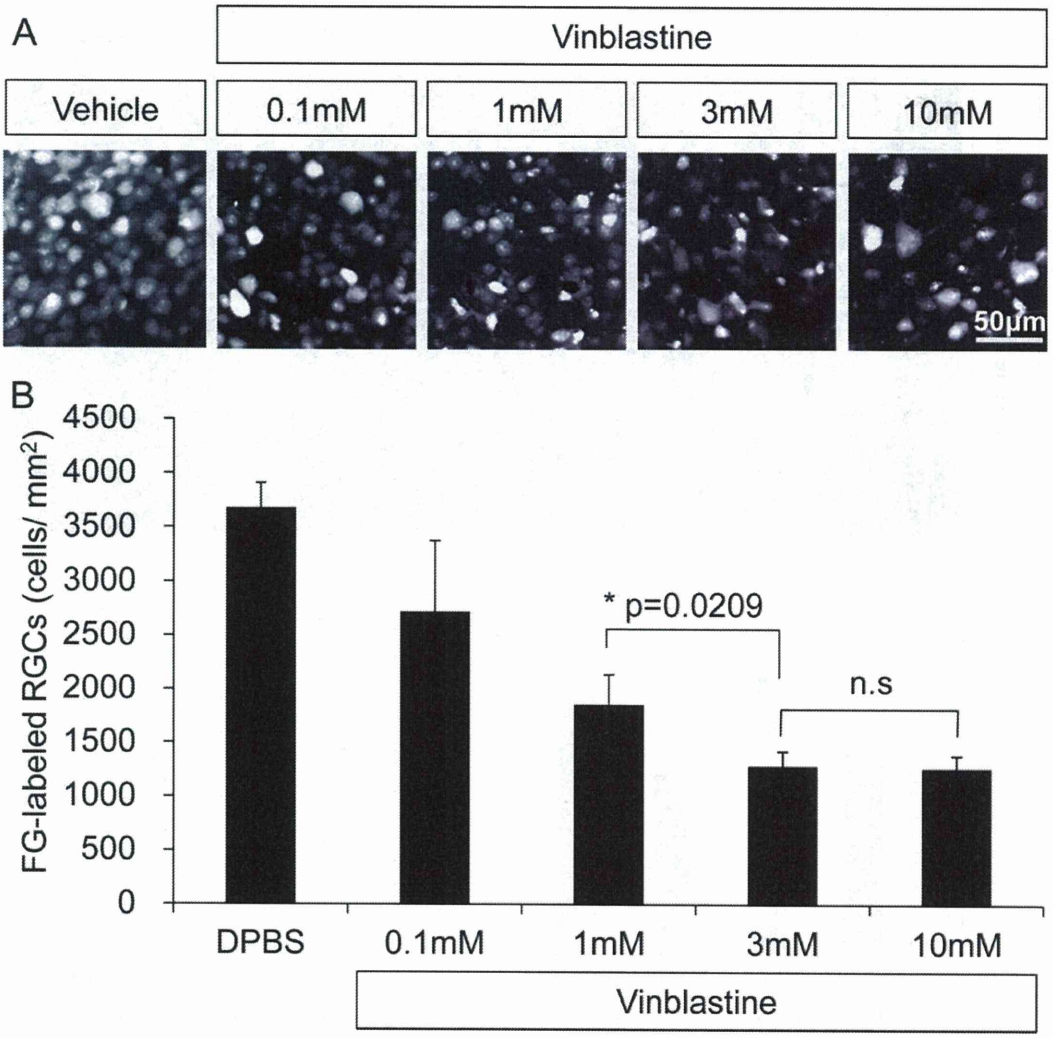

Fig. 4. Dose dependence of vinblastine-induced RGC death. **A:** Representative appearances of FG-labeled RGCs on the flat-mounted retina 7 days after vinblastine treatment at various concentrations (0, 0.1, 1, 3, 10 mM). **B:** Quantitative data on FG-labeled RGC following vinblastine treatment.

compared with the vehicle control (control: 3,623 ± 199 cells/mm^2, 0.1 mM: 2,721 ± 656 cells/mm^2, 1 mM: 1,855 ± 281 cells/mm^2, 3 mM: 1,287 ± 136 cells/mm^2, 10 mM: 1,267 ± 117 cells/mm^2). The RGC density in the 3 mM vinblastine group was significantly lower than that in the 1 mM group ($P = 0.019$). However, there was no significant difference in density noted between the 3 and 10 mM vinblastine groups ($P = 0.631$; Fig. 4B). Therefore, to model axonal injury, 3 mM vinblastine was used for further investigations.

BDNF retrograde transportation blockage is thought to be a trigger for RGC apoptosis (Quigley et al., 2000). Many other studies, including our previous study (Nakazawa et al., 2002), demonstrate that BDNF is a potent neurotrophic factor for RGC survival. We investigated whether intravitreal administration of BDNF could prevent RGC loss in these axonal damage models (Fig. 5A,B). The density of surviving RGCs following axonal injury was significantly higher in the BDNF-treated group than that in the vehicle control group (Fig. 5B; nerve crush without BDNF; 1,153 ± 79 cells/mm^2, nerve crush with BDNF: 1,618 ± 175 cells/mm^2, $P = 0.002$; vinblastine without BDNF: 1,056 ± 104 cells/mm^2, vinblastine with BDNF: 1,477 ± 249 cells/mm^2, $P = 0.001$). Our results indicate that BDNF is neuroprotective for preventing axonal damage-induced RGC death.

Tat-BH4, a potent inhibitor for mitochondria-derived apoptosis, was administered intraperitoneally to investigate the contribution of mitochondria in these

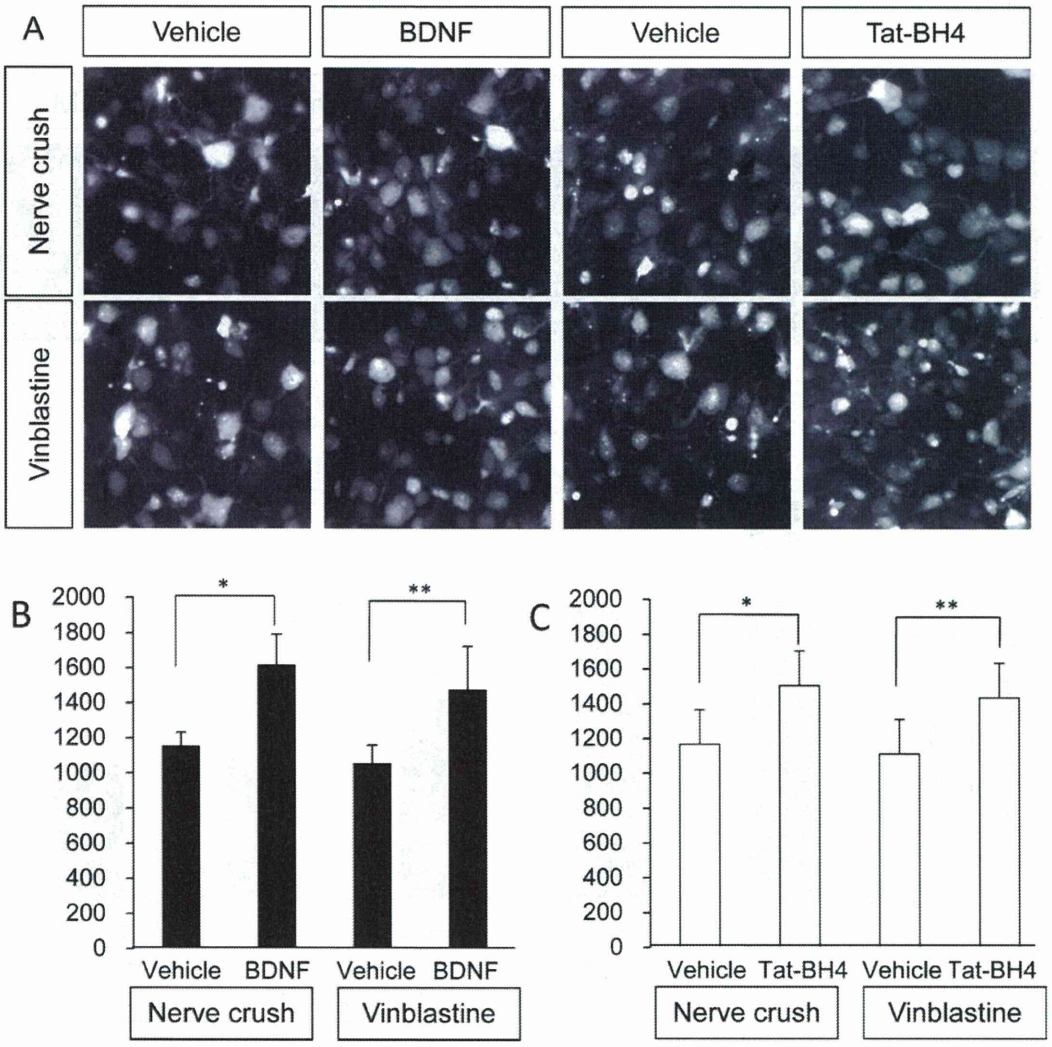

Fig. 5. Brain-derived neurotrophic factor (BDNF) and Tat-BH4 protect RGCs in axonal damage models. **A:** Representative appearances of RGCs on flat mounted retinas. **B:** Quantitative data on the density of RGCs treated with BDNF. **C:** Quantitative data on the density of RGCs treated with Tat-BH4. $*P < 0.05$, $**P < 0.01$.

axonal damage models (Fig. 5A,C). Tat-BH4 is a fusion protein of the protein transduction domain (PTD) from HIV virus and the BH4-domain peptide from Bcl-xL. PTD has the function of transmembrane delivery of proteins or peptides, and the BH4 domain inhibits mitochondrial membrane permeability. Intraperitoneal administration of Tat-BH4 significantly suppressed axonal damage-induced RGC death (nerve crush without Tat-BH4: 1,166 ± 79 cells/mm^2, nerve crush with Tat-BH4: 1,505 ± 139 cells/mm^2, $P < 0.001$; vinblastine without Tat-BH4: 1,112 ± 200 cells/mm^2, vinblastine with Tat-BH4: 1,434 ± 206 cells/mm^2, $P = 0.030$; Fig. 5C). These data suggest that mitochondria-derived signaling is involved in these axonal damage models.

Next we investigated the role of calpain in axonal damage-induced RGC death. Immunoblotting with the antibody for α-fodrin, one of the known calpain substrates, indicated that cleaved α-fodrin (145 kDa) was detectable 3 days after axonal damage either by nerve crush or by vinblastine treatment (Fig. 6). These data suggest that axonal damage induced the fragmentation of α-fodrin as a result of calpain activation in the retina.

Calpastatin (CAST) tightly regulates calpain status, and mice deficient for CAST are susceptible to calpain-dependent neuronal degeneration (Takano et al., 2005). To investigate whether calpain activation following axonal injury was involved in the pathogenesis of RGC death, axonal damage was induced in CAST KO mice.

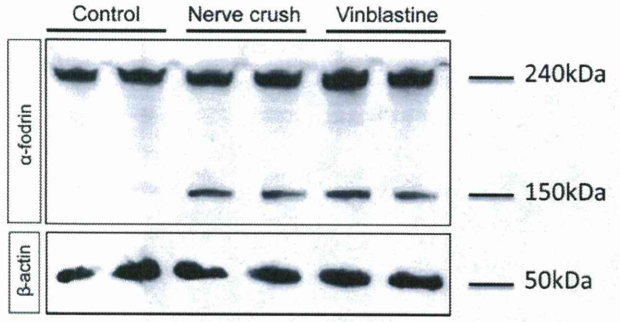

Fig. 6. Cleaved α-fodrin, a calpain substrate, after axonal damage. Representative data on immunoblotting with an antibody for α-fodrin (upper panels), one of the known calpain substrates, and internal control β-actin (lower panels) at day 3 following axonal damage. Note that the cleaved α-fodrin (145 kDa) was detectable with nerve crush or vinblastine treatment.

At first, the densities of RGCs in the uninjured CAST KO mice were not different from those observed in heterozygous and wild-type mice aged between 12 and 24 weeks (Fig. 7A). However, the density of RGCs following nerve crush in CAST KO mice was significantly decreased compared with that observed in wild-type mice (day 3: 3,545 ± 174 cells/mm^2, $P = 0.001$; day 7: 1,153 ± 85 cells/mm^2, $P < 0.001$; day 10: 839 ± 92 cells/mm^2, $P < 0.001$; day 14: 685 ± 110 cells/mm^2, $P < 0.002$; day 28: 488 ± 71 cells/mm^2, $P = 0.006$; Fig. 7B). The trend of susceptibility in CAST KO mice was also evident with the vinblastine treatment (day 3: 2,900 ± 311 cells/mm^2, $P = 0.462$; day 7: 1,266 ± 139 cells/mm^2, $P = 0.001$; day 10: 837 ± 171 cells/mm^2, $P = 0.045$; day 14: 629 ± 101 cells/mm^2, $P = 0.015$; day 28: 570 ± 78 cells/mm^2, $P = 0.007$; Fig. 7C). These data suggest that calpastatin, an endogenous inhibitor, plays a neuroprotective role in the axonal damage-induced RGC.

Next we investigated the therapeutic potential of SNJ-1945, a potent calpain inhibitor, in both in vitro and in vivo systems of RGC injury. In vitro, we administered SNJ-1945 to retinal mixed cells from wild-type mice and CAST KO mice for 24 hr (Fig. 8A). In the vehicle group, the survival rate (RGC/total percentage) of RGCs from the CAST KO mice was significantly lower than that from wild-type mice (wild: 4.2 ± 0.9%, CAST KO: 2.9 ± 0.4%, $P = 0.033$; Fig. 8B). When the retinal mixed culture cells were treated with SNJ-1945 (4 and 40 μM), the survival rate significantly increased, and the difference between wild-type and CAST KO mice vanished. In vivo, orally administered SNJ-1945 significantly delayed RGC death (Fig. 9A) induced by either nerve crush (vehicle: 1,153 ± 85 cells/mm^2, SNJ-1945: 1,650 ± 107 cells/mm^2, $P = 0.002$) or vinblastine treatment (vehicle: 1,299 ± 134 cells/mm^2, SNJ-1945: 1,825 ± 168 cells/mm^2, $P = 0.014$; Fig. 9B) on day 7. According to the results shown in Figure 7B,C, calpain activation in CAST KO mice accelerated the apoptosis of axon-damaged RGCs,

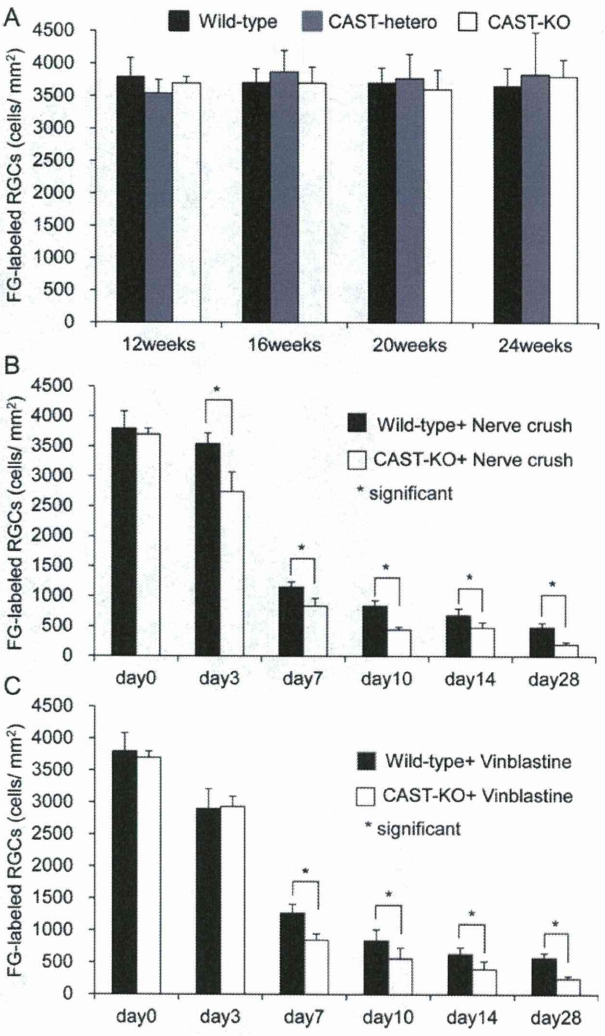

Fig. 7. Susceptibility of calpastatin KO mice to the axonal damage-induced RGC death. **A:** Quantitative data on RGC density without any damage in wild-type, CAST heterozygous, and CAST KO mice between 12 and 24 weeks. **B:** Quantitative data on RGC density damaged by nerve crush. **C:** Quantitative data on RGC density damaged by vinblastine treatment. Note that the susceptibility of CAST KO mice was also evident following nerve crush and vinblastine treatment. *$P < 0.05$.

but the calpain inhibitor could not protect the RGCs after day 14. The retinal transition of orally administered SNJ1945 might be not enough, contracting the neuroprotective effect from day 14. These data suggest that SNJ-1945 has a neuroprotective effect in both in vivo and in vitro models of RGC injury, even in the neurons of the CAST KO mice.

DISCUSSION

This study reveals a critical role for calpain activation in axonal damage-induced RGC death. First, we

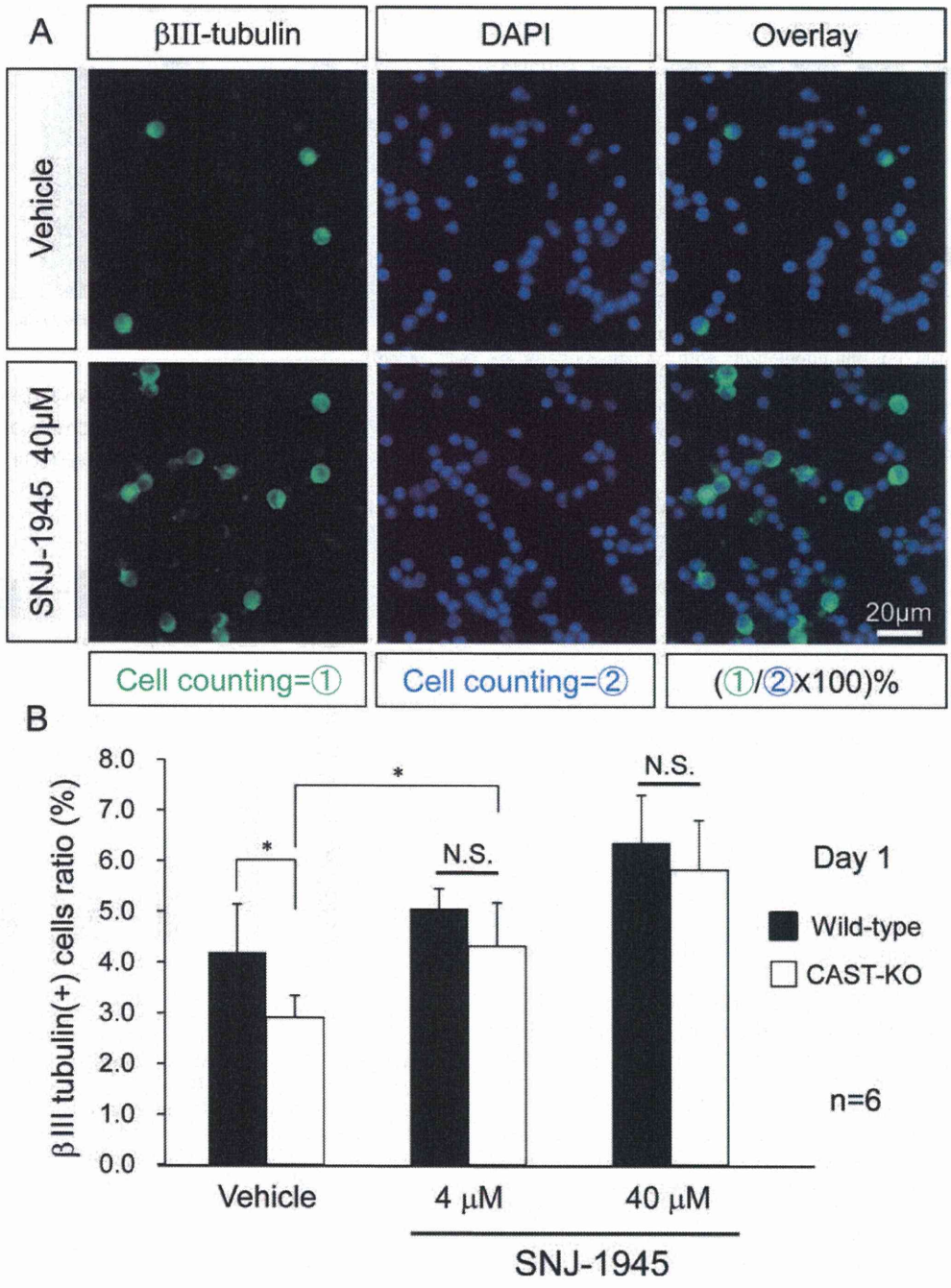

Fig. 8. Neuroprotective effects of SNJ-1945 in the cultured RGCs in vitro. **A:** Representative photographs of ICC with βIII-tubulin, a RGC marker, with (lower panels) or without (upper panels) SNJ-1945 treatment for 24 hr. **B:** Quantitative data on percentage (counting of βIII-tubulin$^+$ RGCs/counting of total DAPI$^+$ cells × 100%) from adult wild-type mice or CAST KO mice with vehicle or SNJ-1945 (4 or 40 mM) on day 1 (24 hr incubated). Note that the susceptibility of CAST KO mice and SNJ-1945 had significant neuroprotective effects in vitro. $*P < 0.05$.

developed a novel model of axonal damage by leaving a gelatin sponge around an optic nerve soaked in vinblastine, a tubulin-disassembly drug. We confirmed that the axoplasmic flow was prevented both in the nerve crush and in the vinblastine models with a double labeling technique. These types of axonal damage induced rapid

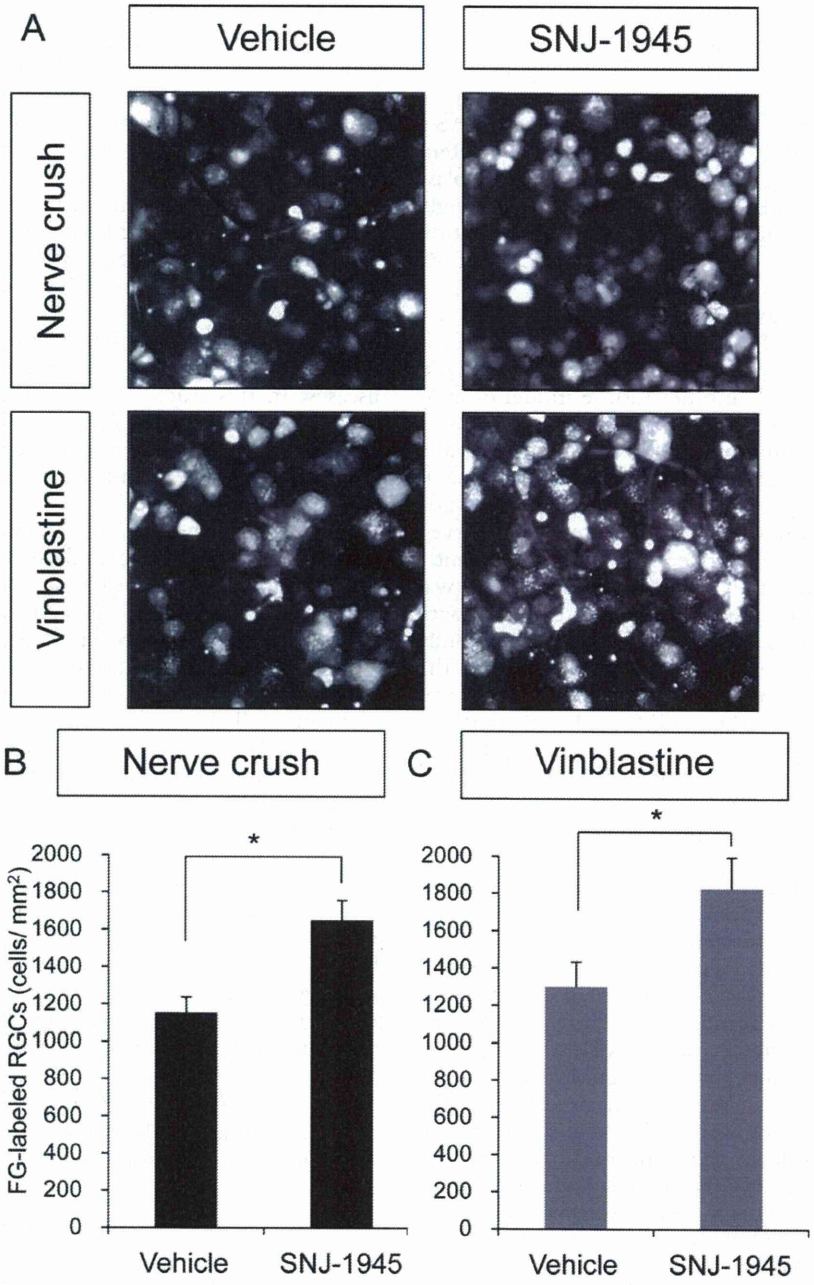

Fig. 9. Neuroprotective effects of SNJ-1945 in the axonal injury-induced RGC death in vivo. **A:** Representative appearances of FG-labeled RGCs on the flat-mounted retina 7 days after nerve crush (upper panels) or vinblastine-treatment (lower panels) with (right panels) or without (left panels) oral administration of SNJ-1945 (100 mg/kg/day). **B:** Quantitative data on FG-labeled RGCs 7 days (upper panels) or 14 days (lower panels) following nerve crush (left panels) and vinblastine treatment (right panels) with or without oral administration of SNJ-1945. Note that SNJ-1945 significantly suppressed RGC death on day 7 induced by either nerve crush or vinblastine treatment. $*P < 0.05$.

RGC loss during the first 7 days in part through a mitochondria-dependent cell death pathway. Using these axonal damage models, we found that calpain was activated in the damaged retina. To investigate whether the calpain activation was involved in the axonal damage-induced RGC death, we induced axonal damage in mice deficient for the calpastatin gene (CAST KO), an endogenous inhibitor protein for calpain. After axonal

damage, the number of surviving FG-labeled RGCs of the CAST KO mice was significantly lower than the number observed in wild-type and heterozygous mice. SNJ-1945, a potent calpain inhibitor, significantly prevented the RGC death in wild-type mice and CAST KO mice in vitro. SNJ-1945 also demonstrated a potent neuroprotective effect against nerve crush- and vinblastine-induced RGC death in vivo. These data strongly suggest that axonal damage-induced calpain activation plays a critical role in axonal damage-induced RGC death.

Nerve crush and axotomy of the optic nerve are often used as models of RGC death to mimic glaucoma or as an experimental model for axon regeneration. Here, we tried to establish another mouse model of axonal damage by preventing axoplasmic flow in the optic nerve. Vinblastine is a microtubule-disassembly drug and has been used in clinical settings for cancer treatment. We left a gelatin sponge soaked with vinblastine at various concentrations around the optic nerve and observed that 10 mM vinblastine destroyed the axon significantly in the treated area, and the axoplasmic flow of FG was almost completely suppressed. After the treatment with vinblastine, the density of surviving RGCs rapidly decreased to approximately 20% of that observed in the untreated control. The time course of RGC death was similar to that of NC-induced RGC death. Furthermore, in these two models of axonal damage, BDNF and Tat-BH4 significantly prevented RGC loss. These data suggest that vinblastine-induced RGC death is a novel model in which the axoplasmic flow of RGC was prevented through a mechanism different from what is observed in traditional mechanical axon damage models, such as nerve crush or axotomy.

Calpastatin is an endogenous inhibitor of calpain. Calpastatin clearly inhibits calpain-dependent proteolysis of cytoskeletal proteins, which results in the prevention of neurodegeneration (Takano et al., 2005). Therefore, we used calpastatin-deficient mice (CAST KO) as a model in which the mice are susceptible in damage-induced calpain activation. We hypothesized that, if the RGCs of CAST KO mice were vulnerable to the axonal damage, we could evaluate the contribution of the calpain-calpastatin pathway to the axonal damage-induced death of RGCs. Interestingly, there was no change in the density of FG-labeled RGCs during the aging process, suggesting that the contribution of calpain was not strong physiologically. On the other hand, orally administered SNJ-1945, a calpain inhibitor, suppressed the activation of calpain pathway in the retina and prevented RGC death in the in vivo mouse model of axonal damage. Taken together, these results demonstrate that the activation of calpain had a strong contribution to the axonal damage-induced RGC death.

Calpain is activated by increased intracellular Ca^{2+}. Ca^{2+} is raised locally through calcium channels and stressed intramitochondrial and endoplasmic reticulum (ER) storage (Azuma and Shearer, 2008). SNJ-1945 was able to inhibit calpain-1 (IC50 = 62 nM) and calpain-2 (45 nM), and orally administered SNJ-1945 (10 mg/kg) accumulated in the retinal tissue at 300 nM (1 hr, at peak) and 100 nM (8 hr; Shirasaki et al., 2006). The data suggest that oral administration allowed SNJ-1945 penetration into the neural retina and that the concentration was enough for the inhibition of calpain-1 and calpain-2.

Axonal and dendritic degeneration, including synapse degeneration, precedes cell body death in CNS diseases such as Alzheimer's disease, Parkinson's disease, Creutzfeldt-Jakob disease, HIV dementia, and multiple sclerosis (Coleman, 2005; Stys, 2005; Koike et al., 2008). Hence, an axonoprotection strategy is required for the treatment of patients suffering from chronic CNS diseases. In this study, we found a significant protective effect against axon degeneration-induced RGC death, suggesting that SNJ-1945 is a strong potential drug candidate for the treatment of diseases sharing a similar pathogenesis.

In retinal diseases, the calpain pathway has been shown to be involved in ischemia (Azuma and Shearer, 2008), glutamate excitotoxicity (Nakazawa et al., 2009; Shimazawa et al., 2010), glaucoma (Huang et al., 2010; Qu et al., 2010), photoreceptor degeneration (Mizukoshi et al., 2010; Paquet-Durand et al., 2010), and diabetic retinopathy (Harris et al., 2006). Furthermore, SNJ-1945 attenuates cell death in cultured human retinal endothelial cells (Ma et al., 2009). Based on our data, SNJ-1945 has therapeutic potential as a new intervention not only for axonopathy but also for treatment of pathological retinal diseases.

In conclusion, orally administered SNJ-1945 successfully reversed axonal damage-induced RGC loss in vivo. Suppression of calpain activation is an important strategy for preventing axonal damage-induced RGC death. These findings suggest that SNJ-1945 is a novel potential therapeutic drug that could be used in the treatment of vision-threatening diseases, such as glaucoma and diabetic axonal atrophy.

ACKNOWLEDGMENTS

We thank Mr. Jiro Watanabe and Koutaro Yamamoto for technical assistance.

REFERENCES

Ambati J, Chalam KV, Chawla DK, D'Angio CT, Guillet EG, Rose SJ, Vanderlinde RE, Ambati BK. 1997. Elevated gamma-aminobutyric acid, glutamate, and vascular endothelial growth factor levels in the vitreous of patients with proliferative diabetic retinopathy. Arch Ophthalmol 115:1161–1166.

Anderson DR, Drance SM, Schulzer M. 1998. The effectiveness of intraocular pressure reduction in the treatment of normal-tension glaucoma. Collaborative Normal-Tension Glaucoma Study Group. Am J Ophthalmol 126:498–505.

Azuma M, Shearer TR. 2008. The role of calcium-activated protease calpain in experimental retinal pathology. Surv Ophthalmol 53:150–163.

Bizat N, Hermel JM, Boyer F, Jacquard C, Creminon C, Ouary S, Escartin C, Hantraye P, Kajewski S, Brouillet E. 2003a. Calpain is a major cell death effector in selective striatal degeneration induced in

vivo by 3-nitropropionate: implications for Huntington's disease. J Neurosci 23:5020–5030.

Bizat N, Hermel JM, Humbert S, Jacquard C, Creminon C, Escartin C, Saudou F, Krajewski S, Hantraye P, Brouillet E. 2003b. In vivo calpain/caspase cross-talk during 3-nitropropionic acid-induced striatal degeneration: implication of a calpain-mediated cleavage of active caspase-3. J Biol Chem 278:43245–43253.

Camins A, Verdaguer E, Folch J, Pallas M. 2006. Involvement of calpain activation in neurodegenerative processes. CNS Drug Rev 12:135–148.

Chatterjee PK, Todorovic Z, Sivarajah A, Mota-Filipe H, Brown PA, Stewart KN, Mazzon E, Cuzzocrea S, Thiemermann C. 2005. Inhibitors of calpain activation (PD150606 and E-64) and renal ischemia-reperfusion injury. Biochem Pharmacol 69:1121–1131.

Chiu K, Lam TT, Ying Li WW, Caprioli J, Kwong Kwong JM. 2005. Calpain and N-methyl-D-aspartate (NMDA)-induced excitotoxicity in rat retinas. Brain Res 1046:207–215.

Coleman M. 2005. Axon degeneration mechanisms: commonality amid diversity. Nat Rev Neurosci 6:889–898.

Deng J, Wu DZ, Gao R. 2000. Detection of glutamate and gamma-aminobutyric acid in vitreous of patients with proliferative diabetic retinopathy. Yan Ke Xue Bao 16:199–202.

Guttmann RP, Sokol S, Baker DL, Simpkins KL, Dong Y, Lynch DR. 2002. Proteolysis of the N-methyl-D-aspartate receptor by calpain in situ. J Pharmacol Exp Ther 302:1023–1030.

Harris F, Biswas S, Singh J, Dennison S, Phoenix DA. 2006. Calpains and their multiple roles in diabetes mellitus. Ann N Y Acad Sci 1084:452–480.

Heijl A, Leske MC, Bengtsson B, Hyman L, Hussein M. 2002. Reduction of intraocular pressure and glaucoma progression: results from the Early Manifest Glaucoma Trial. Arch Ophthalmol 120:1268–1279.

Higuchi M, Tomioka M, Takano J, Shirotani K, Iwata N, Masumoto H, Maki M, Itohara S, Saido TC. 2005. Distinct mechanistic roles of calpain and caspase activation in neurodegeneration as revealed in mice overexpressing their specific inhibitors. J Biol Chem 280:15229–15237.

Huang W, Fileta J, Rawe I, Qu J, Grosskreutz CL. 2010. Calpain activation in experimental glaucoma. Invest Ophthalmol Vis Sci 51:3049–3054.

Huang Y, Wang KK. 2001. The calpain family and human disease. Trends Mol Med 7:355–362.

Iwase A, Suzuki Y, Araie M, Yamamoto T, Abe H, Shirato S, Kuwayama Y, Mishima HK, Shimizu H, Tomita G, Inoue Y, Kitazawa Y. 2004. The prevalence of primary open-angle glaucoma in Japanese: the Tajimi Study. Ophthalmology 111:1641–1648.

Koike T, Yang Y, Suzuki K, Zheng X. 2008. Axon & dendrite degeneration: its mechanisms and protective experimental paradigms. Neurochem Int 52:751–760.

Lam TT, Siew E, Chu R, Tso MO. 1997. Ameliorative effect of MK-801 on retinal ischemia. J Ocul Pharmacol Ther 13:129–137.

Levin LA. 2003. Retinal ganglion cells and neuroprotection for glaucoma. Surv Ophthalmol 48(Suppl 1):S21–S24.

Ma H, Tochigi A, Shearer TR, Azuma M. 2009. Calpain inhibitor SNJ-1945 attenuates events prior to angiogenesis in cultured human retinal endothelial cells. J Ocul Pharmacol Ther 25:409–414.

Marzocco S, Di Paola R, Autore G, Mazzon E, Pinto A, Caputi AP, Thiemermann C, Cuzzocrea S. 2004. Calpain inhibitor I reduces intestinal ischemia-reperfusion injury in the rat. Shock 21:38–44.

Matini P, Moroni F, Lombardi G, Faussone-Pellegrini MS. 1997. Ultrastructural and biochemical studies on the neuroprotective effects of excitatory amino acid antagonists in the ischemic rat retina. Exp Neurol 146:419–434.

McKernan DP, Guerin MB, O'Brien CJ, Cotter TG. 2007. A key role for calpains in retinal ganglion cell death. Invest Ophthalmol Vis Sci 48:5420–5430.

Mizukoshi S, Nakazawa M, Sato K, Ozaki T, Metoki T, Ishiguro S. 2010. Activation of mitochondrial calpain and release of apoptosis-inducing factor from mitochondria in RCS rat retinal degeneration. Exp Eye Res 91:353–361.

Nakazawa T, Tamai M, Mori N. 2002. Brain-derived neurotrophic factor prevents axotomized retinal ganglion cell death through MAPK and PI3K signaling pathways. Invest Ophthalmol Vis Sci 43:3319–3326.

Nakazawa T, Shimura M, Endo S, Takahashi H, Mori N, Tamai M. 2005. N-methyl-D-aspartic acid suppresses Akt activity through protein phosphatase in retinal ganglion cells. Mol Vis 11:1173–1182.

Nakazawa T, Nakazawa C, Matsubara A, Noda K, Hisatomi T, She H, Michaud N, Hafezi-Moghadam A, Miller JW, Benowitz LI. 2006. Tumor necrosis factor-alpha mediates oligodendrocyte death and delayed retinal ganglion cell loss in a mouse model of glaucoma. J Neurosci 26:12633–12641.

Nakazawa T, Hisatomi T, Nakazawa C, Noda K, Maruyama K, She H, Matsubara A, Miyahara S, Nakao S, Yin Y, Benowitz L, Hafezi-Moghadam A, Miller JW. 2007a. Monocyte chemoattractant protein 1 mediates retinal detachment-induced photoreceptor apoptosis. Proc Natl Acad Sci U S A 104:2425–2430.

Nakazawa T, Takahashi H, Nishijima K, Shimura M, Fuse N, Tamai M, Hafezi-Moghadam A, Nishida K. 2007b. Pitavastatin prevents NMDA-induced retinal ganglion cell death by suppressing leukocyte recruitment. J Neurochem 100:1018–1031.

Nakazawa T, Shimura M, Mourin R, Kondo M, Yokokura S, Saido TC, Nishida K, Endo S. 2009. Calpain-mediated degradation of G-substrate plays a critical role in retinal excitotoxicity for amacrine cells. J Neurosci Res 87:1412–1423.

Nath R, Raser KJ, Stafford D, Hajimohammadreza I, Posner A, Allen H, Talanian RV, Yuen P, Gilbertsen RB, Wang KK. 1996. Non-erythroid alpha-spectrin breakdown by calpain and interleukin 1 beta-converting-enzyme-like protease(s) in apoptotic cells: contributory roles of both protease families in neuronal apoptosis. Biochem J 319:683–690.

Paquet-Durand F, Sanges D, McCall J, Silva J, van Veen T, Marigo V, Ekstrom P. 2010. Photoreceptor rescue and toxicity induced by different calpain inhibitors. J Neurochem 115:930–940.

Patrick GN, Zukerberg L, Nikolic M, de la Monte S, Dikkes P, Tsai LH. 1999. Conversion of p35 to p25 deregulates Cdk5 activity and promotes neurodegeneration. Nature 402:615–622.

Qu J, Wang D, Grosskreutz CL. 2010. Mechanisms of retinal ganglion cell injury and defense in glaucoma. Exp Eye Res 91:48–53.

Quigley HA. 1996. Number of people with glaucoma worldwide. Br J Ophthalmol 80:389–393.

Quigley HA, McKinnon SJ, Zack DJ, Pease ME, Kerrigan-Baumrind LA, Kerrigan DF, Mitchell RS. 2000. Retrograde axonal transport of BDNF in retinal ganglion cells is blocked by acute IOP elevation in rats. Invest Ophthalmol Vis Sci 41:3460–3466.

Resnikoff S, Pascolini D, Etya'ale D, Kocur I, Pararajasegaram R, Pokharel GP, Mariotti SP. 2004. Global data on visual impairment in the year 2002. Bull WHO 82:844–851.

Sheppard A, Wu J, Rutishauser U, Lynch G. 1991. Proteolytic modification of neural cell adhesion molecule (NCAM) by the intracellular proteinase calpain. Biochim Biophys Acta 1076:156–160.

Shimazawa M, Suemori S, Inokuchi Y, Matsunaga N, Nakajima Y, Oka T, Yamamoto T, Hara H. 2010. A novel calpain inhibitor, ((1S)-1-((((1S)-1-benzyl-3-cyclopropylamino-2,3-di-oxopropyl)amino)carbonyl)-3-methylbutyl)carbamic acid 5-methoxy-3-oxapentyl ester (SNJ-1945), reduces murine retinal cell death in vitro and in vivo. J Pharmacol Exp Ther 332:380–387.

Shirasaki Y, Yamaguchi M, Miyashita H. 2006. Retinal penetration of calpain inhibitors in rats after oral administration. J Ocul Pharmacol Ther 22:417–424.

Simpkins KL, Guttmann RP, Dong Y, Chen Z, Sokol S, Neumar RW, Lynch DR. 2003. Selective activation induced cleavage of the NR2B subunit by calpain. J Neurosci 23:11322–11331.

Stys PK. 2005. General mechanisms of axonal damage and its prevention. J Neurol Sci 233:3–13.

Suzuki Y, Iwase A, Araie M, Yamamoto T, Abe H, Shirato S, Kuwayama Y, Mishima HK, Shimizu H, Tomita G, Inoue Y, Kitazawa Y. 2006. Risk factors for open-angle glaucoma in a Japanese population: the Tajimi Study. Ophthalmology 113: 1613–1617.

Takano J, Tomioka M, Tsubuki S, Higuchi M, Iwata N, Itohara S, Maki M, Saido TC. 2005. Calpain mediates excitotoxic DNA fragmentation via mitochondrial pathways in adult brains: evidence from calpastatin mutant mice. J Biol Chem 280:16175–16184.

Weinreb RN, Khaw PT. 2004. Primary open-angle glaucoma. Lancet 363:1711–1720.

Wu HY, Tomizawa K, Oda Y, Wei FY, Lu YF, Matsushita M, Li ST, Moriwaki A, Matsui H. 2004. Critical role of calpain-mediated cleavage of calcineurin in excitotoxic neurodegeneration. J Biol Chem 279: 4929–4940.

Clinical Ophthalmology

Dovepress
open access to scientific and medical research

Open Access Full Text Article

ORIGINAL RESEARCH

Reproducibility of retinal circulation measurements obtained using laser speckle flowgraphy-NAVI in patients with glaucoma

Naoko Aizawa
Yu Yokoyama
Naoki Chiba
Kazuko Omodaka
Masayuki Yasuda
Takaaki Otomo
Masahiko Nakamura
Nobuo Fuse
Toru Nakazawa

Department of Ophthalmology, Tohoku University Graduate School of Medicine Sendai, Miyagi, Japan

Background: Laser speckle flowgraphy (LSFG) enables noninvasive quantification of the retinal circulation in glaucoma patients. In this study, we tested the intrasession reproducibility of LSFG-NAVI, a modified LSFG technique.

Methods: Sixty-five eyes from 33 subjects (male (M):female (F) = 17:16) with a mean age of 49.4 ± 11.2 years were examined in this study. Two parameters indicating reproducibility – the coefficient of variation (COV) and the intraclass correlation coefficient (ICC) – were analyzed three times on the same day that mean blur rate (MBR) was measured using LSFG-NAVI. The sites analyzed were the retinal artery and vein, the optic disk, and the choroid. Following classification according to the Glaucoma Hemifield Test (GHT; SITA-Standard 30-2 program), the COV and ICC were examined in patients with (GHT+; 38 eyes, M:F = 20:18, average age 48.9 ± 12.8 years) and without (GHT–; 27 eyes, M:F = 13:14, average age 50.1 ± 8.7 years) abnormal glaucomatous visual fields.

Results: For all subjects, the intrasession reproducibility of MBR in the optic disk (COV: 3.4 ± 2.0; ICC: 0.95) and choroid (COV: 4.7 ± 3.4; ICC: 0.98) was excellent. The reproducibility for the retinal vein (COV: 8.4 ± 5.6, ICC: 0.90) and retinal artery (COV: 10.9 ± 9.9, ICC: 0.9) was moderate. MBRs in the optic disk had good reproducibility in both the GHT+ group (COV: 3.8 ± 2.0; ICC: 0.97) and the GHT– group (COV: 2.9 ± 2.1; ICC: 0.95). Local assessment of the optic disk in normal or glaucoma patients showed that the COVs of the quadrant optic disk areas were best in the temporal area of MBR (3.4%, 4.2%, respectively).

Conclusion: LSFG-NAVI showed favorable reproducibility in evaluation of retinal circulation of glaucoma patients, particularly in the optic disk and choroid.

Keywords: ocular circulation, reproducibility, optic nerve, retina

Introduction

Glaucoma affects more than 70 million people worldwide[1,2] and is the second most frequent cause of blindness.[1] The increase in lifespan worldwide has increased the number of individuals presenting with glaucoma and blindness.[3] Although the pathogenesis of glaucoma remains unclear, one population-based study has suggested that the important risk factors for glaucoma are intraocular pressure (IOP), senescence, and myopia.[4] Other factors such as vascular components may also contribute to optic nerve damage in glaucoma. An increasing body of evidence suggests that dysfunction of ocular microcirculation in the optic nerve influences the progression of glaucoma.[5–7] The association between the degree of optic nerve damage and the defect area has also been demonstrated using fluorescein angiography (FAG).[8–12] Decreased microcirculation in the optic nerve induced by intravitreal administration of endothelin-1 in the

Correspondence: Toru Nakazawa
Department of Ophthalmology, Tohoku University Graduate School of Medicine, 1-1 Seiryo-machi, Aoba-ku, Sendai, Miyagi 980-8574, Japan
Tel +81 22 717 7294
Fax +81 22 717 7298
Email ntoru@oph.med.tohoku.ac.jp

submit your manuscript | www.dovepress.com
Dovepress
http://dx.doi.org/10.2147/OPTH.S22093

optic nerve has been shown to cause cupping in rabbits.[13] These data suggest that disturbance of the microcirculation in the optic nerve head is related to the severity and progression of glaucoma.

As described above, microcirculation was examined using FAG, but it is difficult to quantify changes in microcirculation. Recently, devices that measure ocular circulation have become available. These devices assess the relationship between quantitative retinal or retrobulbar circulation and visual function using scanning laser Doppler flowmetry (SLDF)[14] and color Doppler imaging.[15,16] Although they enable quantification of ocular circulation, it is difficult to capture the same place and reproduce the same image because of the small capture area. By contrast, laser speckle flowgraphy (LSFG) allows for noninvasive quantification of the microcirculation in the optic disk, choroid, and retinal vessels separately in living eyes.[17] The machine is equipped with a fundus camera, a diode laser, an image sensor, an infrared charge-coupled device (CCD) camera, and a high-resolution digital CCD camera. Squared blur rate (SBR), a parameter that yields a theoretically exact measurement of retinal microcirculation, is proportional to blood velocity and showed good correlation with blood flow parameters when measured with other instruments that assess the ocular blood flow.[14,18] With LSFG, 5 seconds are needed to acquire images of the ocular circulation. The images are analyzed and the three sets of heartbeat data are combined to form a single color map depicting the distribution of the retinal circulation. The LSFG method is therefore suitable for monitoring the time course of changes in tissue circulation at the same site in the same eye at various intervals, ranging from seconds to months.[14,17,19–22] In January 2008, LSFG-NAVI, a modified version of LSFG, was approved for use in Japan (Softcare Ltd, Fukuoka, Japan). In the LSFG-NAVI, the parameter was used with mean blur rate (MBR) with the newer CCD camera and the relationship between MBR and SBR was "MBR = 2 × SBR".[23] Recently some studies utilizing MBR for the evaluation of blood flow were reported.[24,25]

There have been no reports on the reproducibility of LSFG-NAVI. Reproducibility of any diagnostic instrument is important both for achieving diagnostic accuracy and for monitoring changes due to disease. The reproducibility of the Heidelberg Retina Tomograph (HRT)[26] and the Stratus OCT[27–30] has been confirmed in the literature, and these measures are considered clinically useful measures of glaucoma progression. Additional studies testing the reproducibility of MBR in normal subjects or glaucoma patients are needed before the LSFG-NAVI can be safely used as a tool for diagnosing and monitoring glaucoma. The purpose of this study was to test the reproducibility of ocular circulation measurements using LSFG-NAVI to determine intrasession reproducibility.

Methods

Patient eligibility

To evaluate intrasession reproducibility, we classified the patients into two groups using the Glaucoma Hemifield Test (GHT). Patients were categorized as within normal limits (control patients, GHT−) or outside normal limits (glaucoma patients, GHT+). The MBRs from the GHT+ patients (38 eyes; M:F = 20:18; average age 48.9 ± 12.8 years) and GHT− patients (27 eyes; M:F = 13:14; average age 50.2 ± 8.7 years) were used for analysis (Table 1). Twenty-four GHT+ patients were on topical antiglaucoma treatment. Glaucoma was diagnosed as glaucomatous optic neuropathy with corresponding glaucomatous visual field loss according to the Anderson–Pattela classification as follows: (1) a GHT outside normal limits; (2) a cluster of three or more non-edge points in a location typical of glaucoma, all of which are significantly lower on the pattern deviation plot at a $P < 0.05$ level and one that is lower at a $P < 0.01$ level; and (3) a corrected pattern standard deviation that is

Table 1 Demographic data for patients with or without glaucoma

	GHT+ (n = 38)	GHT− (n = 27)	*P* value
Number of subjects	38	27	
Age (years)	48.9 ± 12.8	50.2 ± 8.7	0.60
Gender (males:females)	20/18	14/13	0.95
Visual acuity (logMAR)	−0.02 ± 0.15	−0.06 ± 0.06	0.41
Spherical equivalent (D)	−4.2 ± 2.7	−3.8 ± 2.8	0.59
MD (dB)	−7.2 ± 7.2	−0.4 ± 1.4	<0.0001
Intraocular pressure (mmHg)	17.1 ± 3.4	17.5 ± 5.2	0.69
Systolic blood pressure (mmHg)	123.1 ± 14.7	125.1 ± 13.8	0.28
Diastolic blood pressure (mmHg)	74.5 ± 14.2	74.0 ± 12.3	0.88
Heart rate (per minutes)	73.6 ± 11.0	70.2 ± 9.9	0.23

significant at the $P < 0.05$ level. Automated perimetry was performed with a Swedish interactive threshold algorithm (SITA)-standard strategy from the 30-2 program of the Humphrey Field Analyzer (Carl Zeiss Meditec, Dublin, CA). Reliability criteria included fixation losses and false-positive and false-negative rates of less than 20%. Patients were excluded if ocular diseases other than open-angle glaucoma were present, if systemic diseases affecting the visual fields were present, or if they had undergone intraocular surgery.

The procedures used conformed to the Principles of the Declaration of Helsinki, and approval for the analysis of the data was obtained from the Institutional Review Board of the Tohoku Graduate School of Medicine.

Laser speckle flowgraphy

Ophthalmic examinations including slit-lamp biomicroscopy, fundus evaluation, and Goldmann applanation tonometry were performed. After the examination, the pupils of each subject were dilated with 0.5% tropicamide and 0.5% phenylephrine hydrochloride. Blood pressure and IOP were measured after patients had rested for 10 minutes in a sitting position in a dark room, and then ocular circulation was assessed using LSFG-NAVI. To determine intrasession reproducibility, LSFG was performed three times within 10 minutes. The position of each subject's face was reset on the head holder for each examination. The centre of the captured image was set as the midpoint between the optic disk and the macula (Figure 1A and B). Previous eye position was recorded using LSFG Measure (v 6.64.00; Softcare Ltd, Kyushu, Japan), which enabled us to capture the same area in the following examination. In addition, LSFG-NAVI allowed the investigator to adjust the focus by looking at the live-capture image. If the focus of the image was not satisfactory, horizontal dark lines appeared on the live image. Three parameters of the MBR in the optic disk were calculated by the LSFG Analyzer software (v 3.0.47; Softcare Ltd, Kyushu, Japan). After we had identified the margin of the optic disk by hand using a round band, the software segmented out the vessel using the automated definitive threshold and analysis of all the mean of the MBRs (AM), the vessel mean (VM), and the tissue mean (TM) (Figure 1C). These parameters were also calculated for the quadrant area of the superior (S), inferior (I), temporal (T), and nasal areas (N) of the optic disk (Figure 1D). For the analysis of retinal arteries, retinal veins, and choroids, we used the rectangular band (Figure 1B). For accurate sampling of retinal arteries and retinal veins, it is better to set the region of interest (ROI) to more than 1000 pixels and place it on the vessel, avoiding inclusion of the nonvessel tissue. For analysis of the choroid, a square ROI (150 × 150 pixels) was set at one disk diameter away from the temporal margin of the disk without including the main retinal vessels (Figure 1B). All ROI positions were saved and used on the same patient for subsequent analyses.

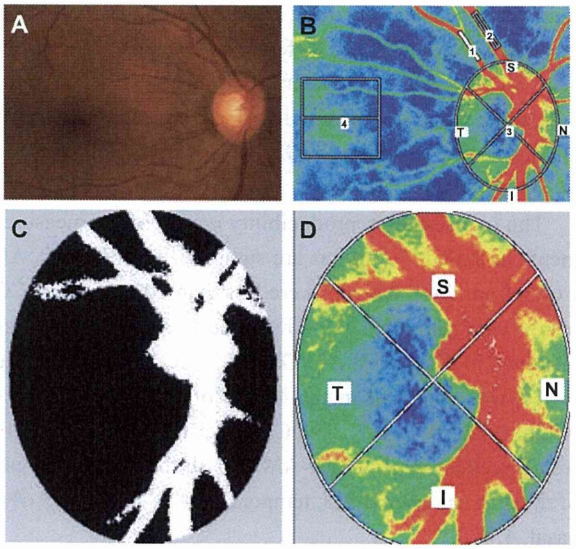

Figure 1 Representative photographs of a glaucoma patient in this study. (**A**) Photograph of the fundus. (**B**) A representative color map produced using LSFG (1, retinal artery; 2, retinal vein; 3, optic disk; 4, choroid). (**C**) Representative binary format images for segmentation between the vessel (white area) and tissue (black area), obtained using image viewer software with an automated definitive threshold. (**D**) Orientation of the quadrant assessment for the MBR in the optic disk.

Analysis for reproducibility

Two parameters indicating reproducibility – the coefficient of variation (COV) and the intraclass correlation coefficient (ICC) – were analyzed with the MBRs from LSFG-NAVI of three continuous examinations on the same day. The segments for analysis were set using a color map of the MBRs in the retinal artery (A), retinal vein (V), optic disk, and choroid.

Statistical analyses

Data were analyzed using statistical software Ekuseru-Toukei 2010 (Social Survey Research Information Co, Ltd, Tokyo, Japan). The Mann–Whitney U-test was used to compare two independent groups, and the chi-squared test was used for categorical data. A P-value of <0.05 was considered statistically significant.

Results

The first analysis was based on three examinations of 65 eyes (38 GHT+ eyes and 27 GHT– eyes) performed on the

same day. The data from these examinations are summarized in Table 1. No significant differences in age, gender, visual acuity, or spherical equivalent (SE) were observed; however, there was a significant difference in mean deviation of Humphrey Field Analyzer (GHT+: −7.2 ± 7.2 dB; GHT−: −0.4 ± 1.4 dB; $P < 0.0001$).

The intrasession reproducibility results of the measurements in the GHT− groups are summarized in Table 2. All COVs from these patients were less than 10%, and all ICC results were more than 0.9. The highest reproducibility was observed in the disk-VM (COV: 1.9%; ICC: 0.98), and the lowest was observed in the MBRs of the retinal arteries (COV: 8.7%; ICC: 0.9). The COVs for the disk parameters were excellent in both disk-AM and all the quadrant areas of the disk (inferior, 4.2%; temporal, 3.4%; superior, 3.6%; nasal, 4.7%).

Intrasession reproducibility of the measurements in the GHT+ groups is shown in Table 2. The highest reproducibility was observed in the disk-TM of the optic disk (COV: 2.3%; ICC: 0.98), and the lowest reproducibility was observed in the retinal artery (COV: 12.4%; ICC: 0.82).

In normal subjects, local assessment showed that the COVs of the quadrant optic disk areas were 3.6% in the S-AM, 3.4% in the T-AM, 4.2% in the I-AM, and 4.7% in the N-AM. By contrast, the COVs of optic disk lesions were 6.4% in the S-AM, 4.2% in the T-AM, 5.8% in the I-AM, and 5.1% in the N-AM in the glaucoma patients.

Table 2 Intrasession reproducibility for GHT− and GHT+ subjects

MBR	GHT−		GHT+	
	COV	ICC	COV	ICC
Artery	8.7 ± 4.5	0.90	12.4 ± 12.4	0.82
Vein	6.2 ± 3.5	0.90	10.1 ± 6.3	0.81
Choroid	4.1 ± 3.2	0.98	5.2 ± 3.7	0.95
Disc-AM	2.9 ± 2.1	0.95	3.8 ± 2.0	0.97
Disc-VM	1.9 ± 1.1	0.98	2.6 ± 1.8	0.96
Disc-TM	2.1 ± 1.1	0.97	2.3 ± 1.5	0.98
I-AM	4.2 ± 2.9	0.98	5.8 ± 4.1	0.93
I-VM	2.8 ± 2.0	0.98	3.5 ± 1.9	0.94
I-TM	2.9 ± 2.1	0.97	3.5 ± 2.7	0.96
T-AM	3.4 ± 1.9	0.99	4.2 ± 2.3	0.98
T-VM	2.3 ± 1.2	0.93	4.2 ± 3.8	0.96
T-TM	3.0 ± 2.1	0.98	3.7 ± 2.3	0.97
S-AM	3.6 ± 2.1	0.98	6.4 ± 4.4	0.94
S-VM	2.3 ± 1.3	0.98	3.5 ± 2.8	0.93
S-TM	2.9 ± 2.1	0.96	4.6 ± 2.9	0.95
N-AM	4.7 ± 4.4	0.92	5.1 ± 4.2	0.94
N-VM	2.3 ± 1.7	0.98	2.6 ± 1.9	0.97
N-TM	3.6 ± 2.5	0.92	3.8 ± 3.2	0.95

Abbreviations: AM, mean of all MBRs; COV, coefficient of variation; GHT, Glaucoma Hemifield Test; I, inferior quadrant area of optic disk; ICC, intraclass correlation coefficient; MBR, mean blur rate; N, nasal quadrant area of optic disk; S, superior quadrant area of optic disk; T, temporal quadrant area of optic disk; TM, tissue mean; VM, vessel mean.

Discussion

Reproducibility of any objective devices for assessing glaucoma is important for both diagnosis and monitoring disease progression. A high level of reproducibility is also required for routine use of objective instruments because changes in the retinal microcirculation during the progression of glaucoma are normally small. Here, we used a modified LSFG to assess the microcirculation of the eyes of normal subjects and glaucoma patients.

The intrasession reproducibility of the three datasets captured on the same day was excellent, suggesting high reproducibility in both normal and glaucomatous eyes. In particular, the reproducibility of the measurements of the optic disk and choroid was excellent compared with the other areas of analysis (ie, the retinal artery and vein). The reproducibility of the retinal artery and vein measurements was significantly lower than that for the disk and choroid (Figure 1B). A wider area of analysis was associated with better reproducibility in MBR. In general, reliable reproducibility of the COV was less than 10%, and the results of COVs of the optic disk (GHT−: 2.9%; GHT+: 3.8%) and choroid (GHT−: 4.1%; GHT+: 5.2%) were good. In the previous version of LSFG, the COVs of reproducibility were 11.7% in the optic disk and 8.7% in the choroid. These data suggest that the reproducibility of LSFG-NAVI is significantly improved compared to the previous LSFG.[31]

Comparison of the COVs between GHT− and GHT+ showed that the COVs from the GHT− subjects were generally better than those of GHT+ subjects (Table 2). The COVs in the retinal vein, the I-VM, the S-AM, and the S-TM were high in the GHT+ subjects. In these areas, we should cautiously interpret the MBR data owing to the low degree of reproducibility among glaucoma patients. Hence, these data suggest that the intrasession reproducibility of LSFG was sufficient for evaluating ocular circulation in glaucoma patients in the clinic.

LSFG-NAVI enables evaluation of the MBR of the optic disk locally on the S, T, I, and N quadrants and separately in the vascular and tissue area. Interestingly, we found that the reproducibility of the VM and TM in the optic disk was better than that of the overall optic disk mean (ie, the AM). In normal subjects, local assessment showed that the COVs of the quadrant optic disk areas were best in the T-AM and worst in the N-AM. By contrast, the COVs were best in the T-AM and worst in the S-AM in the glaucoma patients (Table 2).

These data suggest that the reproducibility of the MBR decreased with structural changes due to glaucoma. The values of COVs in the glaucoma patients, however, were still sufficient for the evaluation of MBR in these patients. Upon further analysis of the VM and TM in local areas of the optic disk, the COV was generally better than that in the AM. These data suggest that the separation of the VM and TM in the optic disk was a good strategy for the assessment of disk microcirculation in the context of ocular disease.

There have been several reports on the reproducibility of objective glaucoma instruments. Budenz et al[28,29] tested the reproducibility of retinal nerve fiber layer (RNFL) thickness measurements with Stratus-OCT (Carl Zeiss Meditec). They tested the intrasession variability of measurements between 88 normal subjects and 59 glaucoma patients and found that the ICCs ranged from 0.84 to 0.97 in normal subjects, with a range of COVs from 1.7% (mean RNFL) to 8.2% (nasal quadrant). In glaucomatous eyes, the ICCs ranged from 0.79 to 0.98, with a COV range of 3.7% (mean RNFL) to 11.9% (nasal quadrant). Our results using the LSFG-NAVI suggest that the reproducibility of this instrument was better than that of the Stratus-OCT and that the LSFG-NAVI is a suitable instrument for measuring ocular circulation, with highly reproducible results.

OCT technology has improved significantly over the years, and various OCT devices are commercially available. These objective instruments require a high degree of reproducibility for purposes of glaucoma diagnosis. Menke et al[32] tested the reproducibility of RNFL measurements of the 3D Fourier-Domain OCT in healthy volunteers and demonstrated an improvement in the reproducibility of RNFL measurements. Notably, the LSFG-NAVI analysis software already has the capacity to measure the same position. In general, in this study, the reproducibility of the MBR measurement of the vessels (retinal arteries and veins) was poorer than that for the disk and choroid. This deficit may be due to the small ROI. Furthermore, when the captured image had a small dark spot of vitreous opacity, it was difficult to determine the quality of the results after obtaining the color map of the MBR. To further improve the reproducibility of LSFG, attention should be focused on the chasing eye tracking technology used to follow eye movement, a high-resolution and high-contrast color map, and an index demonstrating the quality of the color map results.

In conclusion, the reproducibility of LSFG-NAVI was sufficient to evaluate the ocular circulation in this modified version of the LSFG owing to the improvement of the focus during capture. Reproducibility is important for the longitudinal assessment of the state of glaucoma patients. We confirmed that LSFG-NAVI had significantly high reproducibility in measuring the microcirculation of the optic disk and choroid in both normal subjects and glaucoma patients. These data suggest that LSFG-NAVI is an effective and objective instrument for monitoring microcirculation. Although the role of microcirculation in glaucoma patients remains unclear, this technology yields highly reproducible results and could be used to explore the role of ocular circulation not only in glaucoma but also in other ocular diseases.

Disclosure

The authors report no conflicts of interest in this work.

References

1. Quigley HA. Number of people with glaucoma worldwide. *Br J Ophthalmol*. 1996;80(5):389–393.
2. Resnikoff S, Pascolini D, Etyàale D, et al. Global data on visual impairment in the year 2002. *Bull World Health Organ*. 2004;82(11):844–851.
3. Le A, Mukesh BN, McCarty CA, Taylor HR. Risk factors associated with the incidence of open-angle glaucoma: the visual impairment project. *Invest Ophthalmol Vis Sci*. 2003;44(9):3783–3789.
4. Suzuki Y, Iwase A, Araie M, et al. Risk factors for open-angle glaucoma in a Japanese population: the Tajimi Study. *Ophthalmology*. 2006;113(9):1613–1617.
5. Caprioli J, Coleman AL. Blood pressure, perfusion pressure, and glaucoma. *Am J Ophthalmol*. 2010;149(5):704–712.
6. Venkataraman ST, Flanagan JG, Hudson C. Vascular reactivity of optic nerve head and retinal blood vessels in glaucoma – a review. *Microcirculation*. 2010;17(7):568–581.
7. Werne A, Harris A, Moore D, BenZion I, Siesky B. The circadian variations in systemic blood pressure, ocular perfusion pressure, and ocular blood flow: risk factors for glaucoma? *Surv Ophthalmol*. 2008;53(6):559–567.
8. Arend O, Remky A, Plange N, Kaup M, Schwartz B. Fluorescein leakage of the optic disc in glaucomatous optic neuropathy. *Graefes Arch Clin Exp Ophthalmol*. 2005;243(7):659–664.
9. Plange N, Kaup M, Huber K, Remky A, Arend O. Fluorescein filling defects of the optic nerve head in normal tension glaucoma, primary open-angle glaucoma, ocular hypertension and healthy controls. *Ophthalmic Physiol Opt*. 2006;26(1):26–32.
10. Plange N, Kaup M, Weber A, Remky A, Arend O. Fluorescein filling defects and quantitative morphologic analysis of the optic nerve head in glaucoma. *Arch Ophthalmol*. 2004;122(2):195–201.
11. Sihota R, Saxena R, Taneja N, Venkatesh P, Sinha A. Topography and fluorescein angiography of the optic nerve head in primary open-angle and chronic primary angle closure glaucoma. *Optom Vis Sci*. 2006;83(7):520–526.
12. Talusan ED, Schwartz B, Wilcox LM Jr. Fluorescein angiography of the optic disc. A longitudinal follow-up study. *Arch Ophthalmol*. 1980;98(9):1579–1587.
13. Sugiyama T, Mashima Y, Yoshioka Y, Oku H, Ikeda T. Effect of unoprostone on topographic and blood flow changes in the ischemic optic nerve head of rabbits. *Arch Ophthalmol*. 2009;127(4):454–459.
14. Yaoeda K, Shirakashi M, Funaki S, Funaki H, Nakatsue T, Abe H. Measurement of microcirculation in the optic nerve head by laser speckle flowgraphy and scanning laser Doppler flowmetry. *Am J Ophthalmol*. 2000;129(6):734–739.
15. Yamazaki Y, Hayamizu F. Comparison of flow velocity of ophthalmic artery between primary open angle glaucoma and normal tension glaucoma. *Br J Ophthalmol*. 1995;79(8):732–734.

16. Yamazaki Y, Drance SM. The relationship between progression of visual field defects and retrobulbar circulation in patients with glaucoma. *Am J Ophthalmol*. 1997;124(3):287–295.
17. Sugiyama T, Araie M, Riva CE, Schmetterer L, Orgul S. Use of laser speckle flowgraphy in ocular blood flow research. *Acta Ophthalmol*. 2010;88(7):723–729.
18. Nagahara M, Tamaki Y, Tomidokoro A, Araie M. In vivo measurement of blood velocity in human major retinal vessels using the laser speckle method. *Invest Ophthalmol Vis Sci*. 2011;52(1):87–92.
19. Tamaki Y, Kawamoto E, Araie M, Eguchi S, Fujii H. An application of laser speckle phenomenon for noninvasive two-dimensional evaluation of microcirculation in ocular fundus – a preliminary report. *Jpn J Ophthalmol*. 1993;37(2):178–186.
20. Tamaki Y, Araie M, Kawamoto E, Eguchi S, Fujii H. Noncontact, two-dimensional measurement of retinal microcirculation using laser speckle phenomenon. *Invest Ophthalmol Vis Sci*. 1994;35(11):3825–3834.
21. Tamaki Y, Araie M, Kawamoto E, Eguchi S, Fujii H. Non-contact, two-dimensional measurement of tissue circulation in choroid and optic nerve head using laser speckle phenomenon. *Exp Eye Res*. 1995;60(4):373–383.
22. Yaoeda K, Shirakashi M, Funaki S, et al. Measurement of microcirculation in optic nerve head by laser speckle flowgraphy in normal volunteers. *Am J Ophthalmol*. 2000;130(5):606–610.
23. Konishi N, Tokimoto Y, Kohra K, Fujii H. New laser speckle flowgraphy system using CCD camera. *Opt Rev*. 2002;9(4):163–169.
24. Watanabe G, Fujii H, Kishi S. Imaging of choroidal hemodynamics in eyes with polypoidal choroidal vasculopathy using laser speckle phenomenon. *Jpn J Ophthalmol*. 2008;52(3):175–181.
25. Liang Y, Downs JC, Fortune B, Cull G, Cioffi GA, Wang L. Impact of systemic blood pressure on the relationship between intraocular pressure and blood flow in the optic nerve head of nonhuman primates. *Invest Ophthalmol Vis Sci*. 2009;50(5):2154–2160.
26. Miglior S, Albe E, Guareschi M, Rossetti L, Orzalesi N. Intra- and interobserver reproducibility in the evaluation of the optic disc by HRT. *Acta Ophthalmol Scand Suppl*. 2002;236:45.
27. Anton A, Castany M, Pazos-Lopez M, Cuadrado R, Flores A, Castilla M. Reproducibility of measurements and variability of the classification algorithm of Stratus OCT in normal, hypertensive, and glaucomatous patients. *Clin Ophthalmol*. 2009;3:139–145.
28. Budenz DL, Chang RT, Huang X, Knighton RW, Tielsch JM. Reproducibility of retinal nerve fiber thickness measurements using the stratus OCT in normal and glaucomatous eyes. *Invest Ophthalmol Vis Sci*. 2005;46(7):2440–2443.
29. Budenz DL, Fredette MJ, Feuer WJ, Anderson DR. Reproducibility of peripapillary retinal nerve fiber thickness measurements with stratus OCT in glaucomatous eyes. *Ophthalmology*. 2008;115(4):661–666. e4.
30. Tzamalis A, Kynigopoulos M, Schlote T, Haefliger I. Improved reproducibility of retinal nerve fiber layer thickness measurements with the repeat-scan protocol using the Stratus OCT in normal and glaucomatous eyes. *Graefes Arch Clin Exp Ophthalmol*. 2009;247(2):245–252.
31. Tamaki Y, Araie M, Tomita K, Nagahara M, Tomidokoro A, Fujii H. Real-time measurement of human optic nerve head and choroid circulation, using the laser speckle phenomenon. *Jpn J Ophthalmol*. 1997;41(1):49–54.
32. Menke MN, Knecht P, Sturm V, Dabov S, Funk J. Reproducibility of nerve fiber layer thickness measurements using 3D fourier-domain OCT. *Invest Ophthalmol Vis Sci*. 2008;49(12):5386–5391.

Clinical Ophthalmology

Dovepress
open access to scientific and medical research

Open Access Full Text Article

ORIGINAL RESEARCH

Association between optic nerve blood flow and objective examinations in glaucoma patients with generalized enlargement disc type

Naoki Chiba
Kazuko Omodaka
Yu Yokoyama
Naoko Aizawa
Satoru Tsuda
Masayuki Yasuda
Takaaki Otomo
Shunji Yokokura
Nobuo Fuse
Toru Nakazawa

Department of Ophthalmology, Tohoku University Graduate School of Medicine, Sendai, Japan

Background: The purpose of this study was to investigate the correlations between microcirculation in the optic disc, average peripapillary retinal nerve fiber layer thickness cupping parameters, and visual field defects in glaucoma patients with the generalized enlargement disc type.

Methods: A total of 38 eyes from 38 glaucoma patients with the generalized enlargement disc type were included. The microcirculation of the optic nerve head was examined with laser speckle flow graphy, and the mean blur rate in all areas, in vessel area, and in tissue area were calculated using the laser speckle flow graphy analyzer software. Average peripapillary retinal nerve fiber layer thickness was measured using Stratus optical coherence tomography, and cupping parameters were accessed using the Heidelberg retina tomograph. The mean deviation in the Humphrey field analyzer (30-2 SITA standard) was analyzed. The correlation between these parameters was evaluated using the Spearman rank correlation coefficient.

Results: The correlation coefficient of mean blur rate in all optic disc area to the average peripapillary retinal nerve fiber layer thickness, vertical C/D, and mean deviation were $r = 0.7546$ ($P < 0.0001$), $r = -0.6208$ ($P < 0.0001$), and $r = 0.6010$ ($P = 0.0001$), respectively. The mean blur rate in tissue area of the optic disc showed $r = 0.7305$ ($P < 0.0001$), $r = -0.6438$ ($P < 0.0001$), and $r = 0.6338$ ($P < 0.0001$).

Conclusion: We found that the mean blur rate in the optic disc was significantly correlated with the average peripapillary retinal nerve fiber layer thickness, vertical C/D, and mean deviation in patients with the generalized enlargement disc type of glaucoma. In particular, the mean blur rate in tissue area was more highly correlated than the vessel area with other results of examination in glaucoma patients with the generalized enlargement disc type.

Keywords: ocular blood flow, optic disc type, laser speckle flowgraphy, function, structure

Introduction

Glaucoma is characterized by optic nerve fiber atrophy, which causes visual field loss[1] and affects over 70 million people worldwide. It is also the second most common cause of blindness.[2,3] In Asia, especially in Japan, normal-tension glaucoma is the major type of open-angle glaucoma,[4,5] and the proportion of patients with normal-tension glaucoma was reportedly four-fold higher than that of high-tension glaucoma patients in a large Japanese-American clinic population.[6] Therefore, when we treat Japanese patients with glaucoma, it is necessary to refer to not only results from multicenter analyses in Western countries but also results from Asian countries. A number of studies have shown that visual field abnormalities are detected only after 20%–50% of the retinal ganglion cells have been lost, as measured by standard automated perimetry.[7–9] The decrease in retinal nerve fiber layer thickness and change in morphology of the

Correspondence: Toru Nakazawa
Department of Ophthalmology, Tohoku University Graduate School of Medicine, 1-1 Seiryo-machi, Aoba-ku, Sendai, Miyagi 980-8574, Japan
Tel +81 22 717 7294
Fax +81 22 717 7298
Email ntoru@oph.med.tohoku.ac.jp

submit your manuscript | www.dovepress.com
Dovepress
http://dx.doi.org/10.2147/OPTH.S22097

optic disc precede the visual field defects in glaucoma.[10–12] Thus, the latest objective instruments, based on laser confocal systems or optical coherence systems,[13–15] are better for the earlier detection of glaucoma. Importantly, the findings of these objective instruments are also correlated with the degree of mean deviations of the Humphrey field analyzer.[16–18] Automated perimetry is now part of standard follow-up for glaucoma, and objective measuring instruments would be more valuable if they could also be used for follow-up.

It is well known that glaucoma is a multifactorial disease.[19] Various shapes of optic discs have also been clinically recognized in patients with glaucoma. Nicolela and Drance classified optic disc appearances into four types, ie, focal ischemic, myopic, senile sclerotic, and generalized enlargement disc types.[20] They found that classifying the optic disc had a variety of benefits for understanding the mechanism of optic neuropathy in glaucoma and for predicting the prognosis of patients with the disease.[21] We used their methodology and found that, in patients with the myopic glaucoma disc type, if the temporal retinal nerve fiber layer thickness was thinner than 38 μm, visual acuity would be decreased due to glaucoma.[22] Furthermore, the association between Heidelberg retina tomograph (HRT) II parameters and impaired visual fields was strong in patients with the generalized enlargement disc type but not in those with the focal ischemic disc type.[23] In addition, we found that patients with severe high-tension glaucoma had a significantly higher proportion of the generalized enlargement disc type of glaucoma. Thus, a study that evaluates patients by disc type may provide informative data.[24]

Among the risk factors for glaucoma, in addition to intraocular pressure, the microcirculation in the optic disc is critical, especially in normal-tension glaucoma.[25] Fluorescein angiography, scanning laser Doppler flowmetry,[26,27] and color Doppler imaging[28,29] have been used in previous studies; however, all of these devices had limitations in accurately quantifying the ocular blood flow. Laser speckle flow graphy (LSFG) allows quantification of the microcirculation of the optic nerve head, choroid, and retinal vessels separately in living eyes with no contact, using the laser speckle phenomenon.[30] The machine is equipped with a fundus camera, a diode laser, an image sensor, an infrared charge-coupled device camera, and a high-resolution digital charge-coupled device camera. The mean blur rate, a parameter representing the retinal microcirculation, is theoretically an exact measurement that is proportional to blood flow velocity, and has been correlated with blood flow measured by older instruments.[27,31] It takes only a few seconds to acquire an image of the ocular circulation. After analysis, the three-heartbeat data are converted into one-heartbeat data. Then a one-color map is formed to show the distribution of the retinal circulation. Thus, the LSFG method is suitable for monitoring the time course of the change in tissue circulation at the same site in the same eye at various intervals, ranging from seconds to months.[27,30,32–35]

In this study, we investigated the extent of correlation between the mean blur rate measured with laser speckle flowgraphy system LSFG-NAVI (Softcare, Ltd, Fukuoka, Japan) and the objective results of other glaucoma examinations (eg, from HRT II) in patients with the generalized enlargement disc type of glaucoma.

Methods and materials

Patient eligibility

Thirty-eight eyes from 38 Japanese adults aged > 40 years (mean age 62.7 ± 8.6 years) with glaucoma of the generalized enlargement disc type were studied. The generalized enlargement disc type was classified according to the system previously described by Nicolela and Drance[20] and in our publications[23,24] (Figure 1). Patients were excluded from the study if they had glaucoma with other types of optic disc patterns, any other ocular diseases, systemic diseases affecting the visual field or blood flow, a history of intraocular surgery, or refractive errors (spherical equivalent up to –4 diopters [D]). Best-corrected visual acuity was measured with a standard Japanese decimal visual acuity chart and converted to logarithm of the minimum angle of resolution (logMAR) units. If both eyes met the inclusion criteria, the eye with the lower mean deviations on the Humphrey field analyzer (Carl Zeiss Meditec, Dublin, CA) was used in the statistical analyses. Baseline intraocular pressure was measured by Goldmann applanation tonometry before treatment, and if the patient's intraocular pressure was more than 21 mmHg with intraocular pressure-lowering eye drops, the case was excluded. Systolic and diastolic blood pressures were recorded before measurement of LSFG, and the ocular perfusion pressure was calculated as ocular perfusion pressure = 2/3 (1/3 systolic blood pressure + 2/3 diastolic blood pressure) – intraocular pressure. The procedures used in this retrospective study followed the tenets of the Declaration of Helsinki and were approved by the Institutional Review Board of the Tohoku Graduate School of Medicine.

Diagnosis

Glaucoma was diagnosed based on the presence of cupping of the optic disc with defects in the corresponding visual field. Visual field defects were categorized as glaucomatous

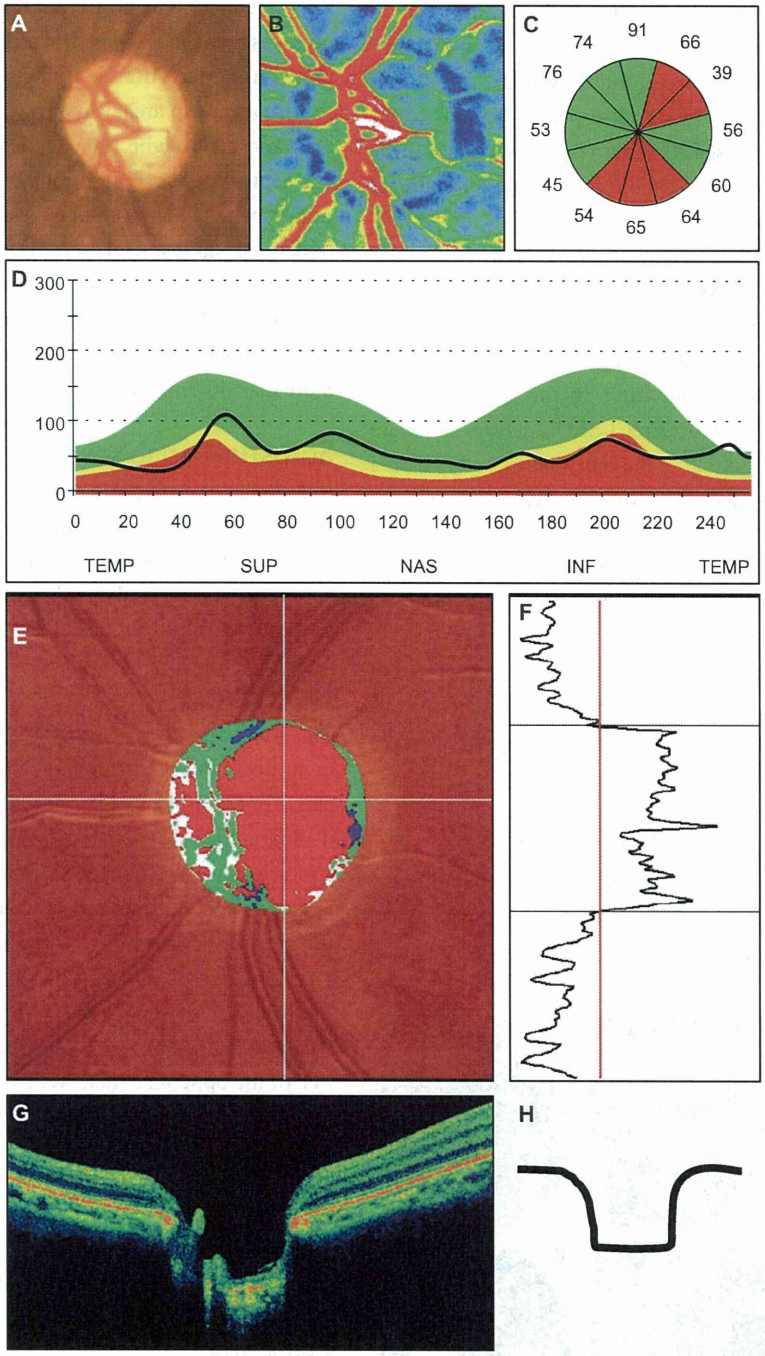

Figure 1 Representative photographs of a patient with the generalized enlargement disc type of glaucoma. (**A**) Fundus photograph of the left optic disc. (**B**) Color map from LSFG-NAVI (Softcare, Ltd, Fukuoka, Japan). (**C**) Average thickness of the retinal nerve fiber layer thickness in the clock area. (**D**) Circumferential retinal nerve fiber layer thickness pattern in a patient with glaucoma. (**E**, **F**) Results of Heidelberg retina tomograph II. (**G**) Vertical section through the center optic nerve by three-dimensional optical coherence tomography.

Abbreviations: TEMP, temporal; SUP, superior; NAS, nasal; INF, inferior.

according to the Anderson-Pattela system if the following criteria were met: the results of the glaucoma hemifield test were outside normal limits; there was a cluster of three or more nonedge points at a location typical for glaucoma, all depressed on the pattern deviation plot at $P < 0.05$, and at least one depressed at $P < 0.01$; and the corrected pattern standard deviation was significant at $P < 0.05$. To evaluate the visual fields, the mean deviation values were obtained

by the Swedish interactive threshold algorithm standard strategy of the 30-2 program of the Humphrey field analyzer. Only the mean deviations of reliable visual field results (<20% fixation errors, <33% false positives, and <33% false negatives) were used. Perimetric data selected for the statistical analyses were those collected within 3 months of the LSFG examination.

Laser speckle flow graphy

To evaluate microcirculation at the optic nerve head, the mean blur rate of the optic disc (Figure 2B) was determined by LSFG-NAVI. Mean blur rates in three areas of the optic disc were calculated using LSFG analyzer software (version 3.0.43.0; Figure 2C); the mean blur rate in all area (MA) of optic disc (disc MA) was the average mean blur rate over the entire optic disc (Figure 2B), mean blur rate in vessel area (MV) of optic disc (disc MV) was average over the vessel area (Figure 2D, white area), and mean blur rate in tissue area of the optic disc (MT) of optic disc (disc MT) was the average of the mean blur rate of the optic disc area minus the vessel area (Figure 2D, black area). These three parameters were measured at the same time, and the averages were used in the statistical analyses.

Measurement of OCT and HRT II

The patients' pupils were dilated before examination. Retinal nerve fiber layer thickness around the optic disc was determined using the Stratus optical coherence tonometer (OCT, Carl Zeiss Meditec), and the average retinal nerve fiber layer thickness was used for analysis. Fifteen HRT parameters were determined using the HRT II (Heidelberg Engineering Inc, CA), ie, disc area, cup area, rim area, cup/disc area ratio, rim/disc area ratio, cup volume, rim volume, mean cup depth, maximum cup depth, height variation contour, cup shape measure, mean retinal nerve fiber layer thickness and cross-sectional area, horizontal cup/disc area ratio, and vertical cup/disc area ratio. The optic disc contour line was manually drawn at the inner edge of the scleral ring by one experienced glaucoma specialist. If the standard deviation of the mean topographic image was more than 40 μm, the data were excluded.

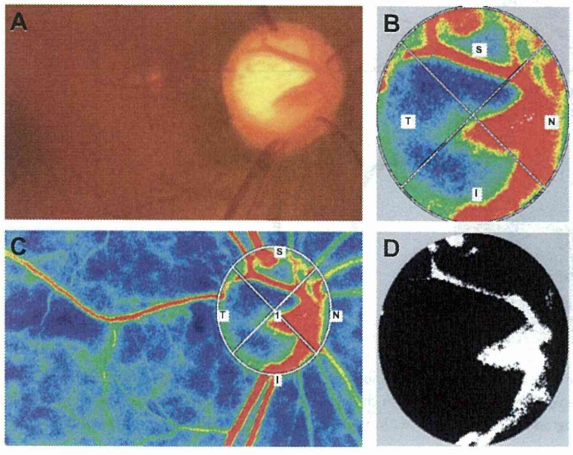

Figure 2 Color map and binary image of laser speckle flow graph in a patient with the generalized enlargement disc type of glaucoma. (**A**) Fundus photograph of the left optic disc in a patient with the generalized enlargement disc type of glaucoma (64-year-old female, baseline intraocular pressure 17 mmHg, Humphrey field analyzer mean deviation –8.01 dB). (**B**) Color map image of the optic nerve head. (**C**) Color map image of the whole area and the optic nerve head depicted by region of interest. (**D**) Binary map of the optic nerve head. The white area indicates the vessel, and the black area indicates tissue.

Statistical analyses

Relationships between LSFG values and degree of alterations, including mean deviation values, retinal nerve fiber layer thickness, and HRT II parameters, were determined by a simple regression analysis. A P value <0.05 was considered to be statistically significant.

Results

This study examined 38 patients with the generalized enlargement disc type of glaucoma, comprising 22 (58%) women and 16 (42%) men, of mean age 62.7 ± 8.6 years. Patient demographic data are listed in Table 1. The average spherical equivalent was –0.67 ± 1.88 D, the average value ± mean deviation on the Humphrey field analyzer was –8.0 ± 6.8 dB, the average peripapillary retinal nerve fiber layer thickness was 71.6 ± 18.4 μm, and the best-corrected visual acuity (logMAR) was 0.032 ± 0.090. The mean values for MA of the optic disc (disc MA), MV of the optic disc (disc MV), and MT of the optic disc (disc MT) were 20.6 ± 5.5, 44.6 ± 2.5,

Table 1 Patient demographic data

Sex (male:female)	22:16
Age (years)	62.7 ± 8.6
Spherical equivalent (D)	–0.67 ± 1.88
HFA-MD (dB)	–8.0 ± 6.8
Baseline IOP (mmHg)	18.2 ± 8.4
BCVA (logMAR)	0.032 ± 0.090
Average RNFLT	71.6 ± 18.4
Disc MA	20.6 ± 5.5
Disc MV	44.6 ± 2.5
Disc MT	11.5 ± 2.1

Note: The data show the means ± standard deviation.
Abbreviations: HFA-MD, Humphrey field analyzer mean deviation; IOP, intraocular pressure; BCVA, best-corrected visual acuity; disc MA, mean blur rate in all area of the optic disc; disc MA, mean blur rate in all area of the optic disc; disc MT, mean blur rate in tissue area of the optic disc; MD, mean deviation of 30-2; HFA, Humphrey field analyzer; RNFLT, retinal nerve fiber layer thickness of Stratus optical coherence tomography.

Table 2 Mean values of HRT II parameters

HRT II parameters	Mean values
Disc area (mm^2)	2.52 ± 0.52
Cup area (mm^2)	1.70 ± 0.51
Rim area (mm^2)	0.82 ± 0.43
Cup/Disc area ratio	0.67 ± 0.15
Rim/Disc area ratio	0.33 ± 0.15
Cup volume (mm^3)	0.65 ± 0.33
Rim volume (mm^3)	0.17 ± 0.14
Mean cup depth (mm)	0.40 ± 0.11
Maximum cup depth (mm)	0.85 ± 0.16
Height variation contour (mm)	0.58 ± 0.37
Cup shape measure	−0.04 ± 0.08
Mean RNFL thickness (mm)	0.11 ± 0.11
RNFL cross-sectional area (mm^2)	0.60 ± 0.68
Horizontal cup/disc ratio	0.84 ± 0.13
Vertical cup/disc ratio	0.81 ± 0.13

Abbreviations: HRT, Heidelberg retina tomograph; RNFL, retinal nerve fiber layer.

and 11.5 ± 2.1, respectively. The average values for the HRT II parameters are listed in Table 2.

The correlation between the disc MA and the Humphrey field analyzer mean deviation was significant (r = 0.6010, $P = 0.0001$), as was the correlation between the disc MA and the average peripapillary retinal nerve fiber layer thickness (r = 0.7546, $P < 0.0001$). These data are listed in Tables 3 and 4. Next, we investigated the correlation between disc mean blur rate and several HRT II parameters (Table 5). Correlations between the disc MA and HRT II parameters were significant for the cup area (r = 0.3637, $P = 0.0248$), rim area (r = 0.5588, $P = 0.0003$), cup/disc area ratio (r = −0.5437, $P = 0.0004$), rim/disc area ratio (r = 0.5437, $P = 0.0004$), cup volume (r = −0.3636, $P = 0.0248$), rim volume (r = 0.3430, $P = 0.0350$), height variation contour (r = −0.4261, $P = 0.0076$), mean retinal nerve fiber layer thickness (r = 0.4096, $P = 0.0106$), cross-sectional retinal nerve fiber layer area (r = 0.4418, $P = 0.0055$), and vertical cup/disc ratio (r = −0.6208, $P < 0.0001$). The correlation was strongest for the vertical cup/disc area ratio.

We used the LSFG analyzer software to measure the mean blur rate in the vessel area and in the tissue area separately. There was a significant correlation between the

Table 3 Relationship between mean blur rate and mean deviation (MD)

	Disc MA		Disc MV		Disc MT	
	r	*P*	*r*	*P*	*r*	*P*
MD	0.6010	0.0001	0.3346	0.0401	0.6338	<0.0001

Abbreviations: disc MA, mean blur rate in all area of the optic disc; disc MA, mean blur rate in all area of the optic disc; disc MT, mean blur rate in tissue area of the optic disc.

Table 4 Relationship between mean blur rate and average RNFLT

	Disc MA		Disc MV		Disc MT	
	r	*P*	*r*	*P*	*r*	*P*
Average of RNFLT	0.7546	<0.0001	0.4825	0.0022	0.7305	<0.0001

Abbreviations: RNFLT, retinal nerve fiber layer thickness; disc MA, mean blur rate in all area of the optic disc; disc MA, mean blur rate in all area of the optic disc; disc MT, mean blur rate in tissue area of the optic disc.

disc MV and the Humphrey field analyzer mean deviation (r = 0.3346, $P = 0.0401$), average peripapillary retinal nerve fiber layer thickness (r = 0.4825, $P = 0.0022$), and vertical cup/disc ratio (r = −0.3226, $P = 0.0482$). However, the disc MT was more strongly associated with the Humphrey field analyzer mean deviation (r = 0.6338, $P < 0.0001$), average peripapillary retinal nerve fiber layer thickness (r = 0.7305, $P < 0.0001$), and vertical cup/disc ratio (r = −0.6438, $P < 0.0001$) than was the disc MV. Interestingly, the disc MT showed stronger correlations with the mean blur rate and the various parameters assessed in the glaucoma examination than did the disc MV.

Discussion

In this study, we investigated whether there were associations between mean blur rate, a new parameter of blood flow determined using LSFG-NAVI, and other traditional parameters used in examination for glaucoma, which included Humphrey field analyzer mean deviation, average peripapillary retinal nerve fiber layer thickness, and HRT II in patients with generalized enlargement disc type glaucoma. We found that the disc MA and disc MT were significantly correlated with values recorded using the Humphrey field analyzer, OCT, and HRT II. The strongest correlation was between the disc MA and the average peripapillary retinal nerve fiber layer thickness (r = 0.7546, $P < 0.0001$). These data suggest that the mean blur rate from LSFG-NAVI is useful as an objective measurement in patients with glaucoma.

We focused on patients with the generalized enlargement disc type of glaucoma. To evaluate the potential of using the mean blur rate from LSFG-NAVI as an objective measure for patients with glaucoma, we needed to compare the mean blur rate values with other parameters used in examination for glaucoma. In a previous study, we found that classification of the optic disc type was beneficial for accurate investigation of the correlation between Humphrey field analyzer mean deviation and other objective instruments used for glaucoma.[23] In that study, the group with the generalized enlargement disc type showed the strongest